

Intersite Coulomb repulsion driven quadrupole instability and magnetic ordering in the orbital frustrated $\text{Ba}_2\text{MgReO}_6$

Xuanye Zhang,^{1,*} Jinyu Zou,^{1,*} and Gang Xu^{1,2,3,†}

¹Wuhan National High Magnetic Field Center & School of Physics,
Huazhong University of Science and Technology, Wuhan 430074, China

²Institute for Quantum Science and Engineering,

Huazhong University of Science and Technology, Wuhan, 430074, China

³Wuhan Institute of Quantum Technology, Wuhan, 430074, China

We develop an unrestricted Hartree-Fock mean-field method including Coulomb interaction U , V and spin orbital coupling λ self-consistently to investigate the mechanism of structural instability and magnetic ordering in $\text{Ba}_2\text{MgReO}_6$. A comprehensive quadrupole phase diagram versus U and V with $\lambda=0.28\text{eV}$ is calculated. Our results demonstrate that, while U and λ mainly lead to the onsite quadrupole $Q_{x^2-y^2}$ and $Q_{3z^2-r^2}$, the intersite Coulomb repulsion V would arrange $Q_{x^2-y^2}$ antiparallely, accompanied with small parallel $Q_{3z^2-r^2}$, and stabilize $\text{Ba}_2\text{MgReO}_6$ into the body-centered tetragonal structure. Such antiparallel $Q_{x^2-y^2}$ provides a new mechanism of Dzyaloshinskii–Moriya interaction, and give rise to the canted antiferromagnetic (CAF) state along [110] axis. Moreover, sizable octupoles such as $O_{21}^{31}, O_{21}^{33}, O_{21}^{34}$ and O_{21}^{36} are discovered for the first time in CAF states. Our study not only provides a comprehensive understanding of the nature and exotic properties in $\text{Ba}_2\text{MgReO}_6$, but also reveal some commonality of 5d compounds.

5d electrons usually have two remarkable characters. One is the dramatically enhanced spin-orbit coupling (SOC) λ originated from the huge atomic number Z . The other is the spatially extended orbit, which could lead to considerable intersite Coulomb repulsion V . In the past decades, the interplay between the energy comparable onsite Coulomb interaction U and SOC λ and its resulting exotic properties in 5d transition metal (TM) compounds have attracted increasing interest, including the SOC assistant Mott metal-insulator transition [1, 2], non-collinear magnetic moment [3–5], orbital frustration (OF) and high-rank multipole [6–11]. Among them, the orbital frustrated honeycomb and face-centered cubic(fcc) lattice magnets have been extensively studied recently, which are reported to host the long-pursuit quantum spin liquid states when the OF maintains and dominates [12, 13], or give rises to lattice distortion accompanied with the orbital ordering (OO) when OF is eliminated [14]. However, while most efforts have been focused on the interplay between U and λ and the resulting properties, rare works pay attention to the influence of V , though it could play a key role to determine the exotic states and properties in 5d TM compounds. Especially in the first-principles calculation field, a generic program to deal with U , V and λ self-consistently is still lacking.

The double perovskite $\text{Ba}_2\text{MgReO}_6$ with $5d^1$ configuration, adopting the frustrated fcc lattice, provides an ideal platform to study the interplay between U , λ and V , as well as the resulting exotic properties [15–22]. $\text{Ba}_2\text{MgReO}_6$ undergoes two phase transitions upon cooling, including cubic–tetragonal phase transition at T_q and canted antiferromagnetic (CAF) phase transition with a small gap at T_m [17–21]. Further synchrotron X-ray diffraction measurements of high-quality single

crystals show the tetragonal distortion is enhanced below T_m , which indicates that quadrupoles are coupled with magnetic orders [18]. Recently, magnetic entropy is obtained by subtracting phonon contribution in heat capacity [21], which reflects the degeneracy of the ground state multiplet $N = 2$ is different from Ref[17]. These evidences imply that pure spin model is not enough to describe the magnetic mechanism in $\text{Ba}_2\text{MgReO}_6$. In fact, strong SOC not only leads to small magnetic dipole ordering, as small as $0.3\mu_B$ in $\text{Ba}_2\text{MgReO}_6$, but also opens up the possibility of high-rank multipoles [7, 9]. Such high-rank multipoles are usually entangled with the magnetic dipole ordering together and hard to be detected by the conventional experiments [23, 24]. Therefore, a comprehensive understanding of the phase transitions and exotic properties in $\text{Ba}_2\text{MgReO}_6$ remains elusive until now.

In this letter, based on first-principles calculations, we develop an unrestricted Hartree-Fock mean-field method included U , λ and V self-consistently to investigate the nature of phase transition and exotic properties in $\text{Ba}_2\text{MgReO}_6$. Our study demonstrates that, while U and λ mainly determine the form of the onsite order parameters such as orbital quadrupoles and magnetic dipoles, the intersite Coulomb repulsion V is crucial to determine the arrangement of these orbital quadrupoles and magnetic dipoles. Our calculations figure out that the antiparallel (AP-) $Q_{x^2-y^2}$ could minimize the intersite Coulomb repulsion mostly. So that small $V=10\text{meV}$ is enough to stabilize $\text{Ba}_2\text{MgReO}_6$ into the body-centered tetragonal structure accompanied with the AP- $Q_{x^2-y^2}$ and small amplitude of parallel $Q_{3z^2-r^2}$ quadrupole. Such quadrupolar state with incompletely quenched orbital angular momentum provides a new mechanism of Dzyaloshinskii–Moriya (DM) interaction, resulting in

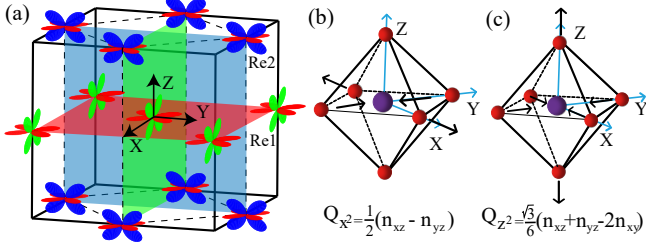


FIG. 1. (a) Schematic of Re1 and Re2 atoms in face-centered-cubic unit cell (solid line) and tetragonal supercell (dotted lines). XY, XZ and YZ orbit (plane) is indicated by red, green and blue color. (b)(c) The oxygen octahedral distortion and orbital order corresponding to Q_{x^2} and Q_{z^2} respectively.

the experimentally observed CAF ground state [17, 18]. Moreover, various magnetic octupoles are discovered in the CAF ground state, where the octupoles have comparable weight with magnetic dipoles and exhibit canted arrangement along z direction. This complex magnetic structure may be the source of abnormal magnetic entropy and weak magnetic anisotropy in the CAF ground state.

As shown in Fig. 1a, $\text{Ba}_2\text{MgReO}_6$ adopts double perovskite structure with $Fm\bar{3}m$ space group [15, 17]. The crystal field of the local oxygen octahedron splits d-orbitals of Re atom into a higher doubly-degenerate e_g orbitals and lower triply-degenerate t_{2g} orbitals [25, 26]. With $5d^1$ configuration, t_{2g} orbitals are enough for low physics of $\text{Ba}_2\text{MgReO}_6$, and the one electron occupation usually leads to spontaneous symmetry breaking with orbital ordering [14, 27–30], which can be expanded by the quadrupolar orders $Q_{x^2-y^2}$ (abbr. Q_{x^2}) and $Q_{3z^2-r^2}$ (abbr. Q_{z^2})

$$\begin{aligned} Q_{x^2-y^2} &= \frac{1}{2}(n_{xz} - n_{yz}) \\ Q_{3z^2-r^2} &= \frac{\sqrt{3}}{6}(n_{xz} + n_{yz} - 2n_{xy}) \end{aligned} \quad (1)$$

Q_{x^2} breaks O_h to D_{2h} and Q_{z^2} breaks to D_{4h} , corresponding to the octahedral distortion shown in Fig. 1b and Fig. 1c respectively.

In order to comprehensively investigate the effects of the interactions, including U, λ and V, on the orbital ordering and physical properties in $\text{Ba}_2\text{MgReO}_6$, we first construct the maximally localized Wannier functions of t_{2g} to obtain H_{tb} , using the Vienna ab initio simulation [31, 32] and WANNIER90 package [33] based on cubic structure with lattice constant $a=8.0802\text{\AA}$ [18]. Then U, λ and V are successively added to calculate the possible orders and corresponding energy, by self-consistent unrestricted Hartree-Fock mean-field method.

We first take the onsite Coulomb repulsion H_U into account, which adopts the form of Kanamori Hamiltonian [34] and has been reported as the driving force

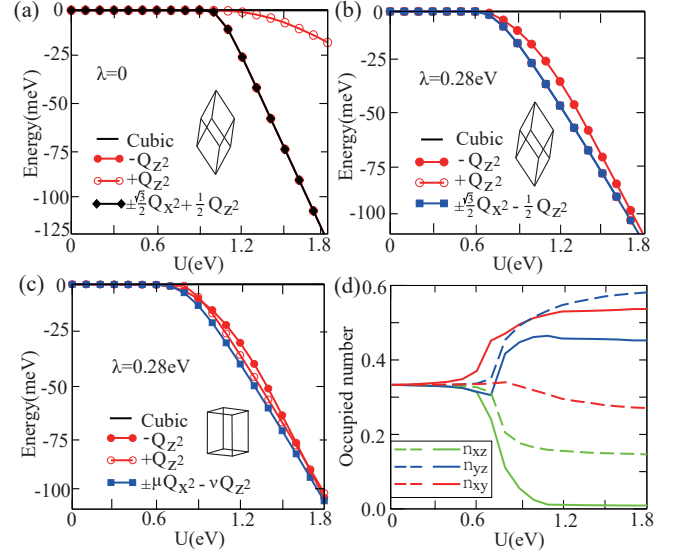


FIG. 2. (a)–(b) Total energy of orbital ordering states without and with $\lambda = 0.28\text{eV}$ relative to the cubic as a function of U. (c) Total energy of orbital ordering states based on tetragonal supercell with $\lambda = 0.28\text{eV}$ relative to the cubic as a function of U. (d) The electron occupation of d_{xy} , d_{xz} and d_{yz} orbitals as a function of U. The dotted line and the solid line represent the situation in AP- $Q_{x^2} + Q_{z^2}$ with $V=50\text{meV}$ and $-\mu Q_{x^2} - \nu Q_{z^2}$ state without V respectively.

of the orbital ordering in many materials [35–39]. The calculated results are shown in Fig. 2a. When $U > 1.0\text{eV}$, three symmetrically equivalent quadrupole states $-Q_{z^2}$ ($n_{xy}=1$), $\frac{\sqrt{3}}{2}Q_{x^2} + \frac{1}{2}Q_{z^2}$ ($n_{xz}=1$) and $-\frac{\sqrt{3}}{2}Q_{x^2} + \frac{1}{2}Q_{z^2}$ ($n_{yz}=1$) emerge spontaneously, which are about dozens meV lower than their counterparts with opposite ordering such as Q_{z^2} . One can understand the result by the mean field total energy of the Kanamori Hamiltonian with time-reversal symmetry (TRS):

$$E = -\frac{U}{4}(Q_{x^2-y^2}^2 + Q_{3z^2-r^2}^2) \quad (2)$$

which gives the energy $-\frac{U}{12}$ for $-Q_{z^2}$ state with $n_{xy} = 1$, lower than the energy of Q_{z^2} state ($-\frac{U}{48}$) with $n_{xz}=n_{yz}=0.5$. Such results demonstrate that the onsite Coulomb repulsion U tends to enforce the electron to occupy one single orbital.

To reveal the effect of SOC on orbital ordering, we further introduce H_{soc} of t_{2g} orbitals [25], where the SOC strength $\lambda=0.28\text{eV}$ is determined by the band structures fitting with first-principles calculations. The results are plotted in Fig. 2b, obviously contrary to the results without SOC (Fig. 2a), and give rise to that Q_{z^2} and $\pm\frac{\sqrt{3}}{2}Q_{x^2} - \frac{1}{2}Q_{z^2}$ orders become more stable, about 10meV lower than $-Q_{z^2}$ state in the regime $0.9\text{eV} < U < 1.5\text{eV}$. The result can be understood by the effect of U in the spin-orbital entangled quartet space

$J_{eff} = 3/2$, which are [25]

$$\begin{aligned}
 \left| J_{eff} = \frac{3}{2}, m = -\frac{3}{2} \right\rangle &= \frac{1}{\sqrt{2}} |d_{yz\downarrow}\rangle - \frac{i}{\sqrt{2}} |d_{xz\downarrow}\rangle \\
 \left| J_{eff} = \frac{3}{2}, m = \frac{3}{2} \right\rangle &= -\frac{1}{\sqrt{2}} |d_{yz\uparrow}\rangle - \frac{i}{\sqrt{2}} |d_{xz\uparrow}\rangle \\
 \left| J_{eff} = \frac{3}{2}, m = -\frac{1}{2} \right\rangle &= \frac{1}{\sqrt{6}} |d_{yz\uparrow}\rangle - \frac{i}{\sqrt{6}} |d_{xz\uparrow}\rangle + \sqrt{\frac{2}{3}} |d_{xy\downarrow}\rangle \\
 \left| J_{eff} = \frac{3}{2}, m = \frac{1}{2} \right\rangle &= -\frac{1}{\sqrt{6}} |d_{yz\downarrow}\rangle - \frac{i}{\sqrt{6}} |d_{xz\downarrow}\rangle + \sqrt{\frac{2}{3}} |d_{xy\uparrow}\rangle
 \end{aligned} \quad (3)$$

It is obvious that $|m = \pm 3/2\rangle$ correspond to Q_{z^2} order while $|m = \pm 1/2\rangle$ correspond to $-Q_{z^2}$ order. The onsite Coulomb repulsion U , through the nearest neighbor hopping, can induce the antiferromagnetic exchange interaction J ($J > 0$) between same orbitals and ferromagnetic exchange interaction J' ($J' < 0$) between orthogonal orbitals, which have the magnitude of $\frac{t^2}{U}$ (about 10 meV). Although the system preserves TRS during the calculations in Fig. 2b, the exchange interaction can play roles through the following TRS invariant two-site Fock states $\Psi_m = |A, m\rangle|B, m\rangle + |A, -m\rangle|B, -m\rangle$ or $\Psi'_m = |A, m\rangle|B, -m\rangle - |A, -m\rangle|B, m\rangle$, with $m = 1/2, 3/2$. We found that while J cannot distinguish the $1/2$ and $3/2$ subspace, J' will make $3/2$ lower. Effectively, the ferromagnetic exchange term can be rewritten as

$$J' S_i^t S_j^t = J' \sum_{\sigma=x,y,z} S_i^{\sigma} S_j^{\sigma} \quad (4)$$

where S_j^t is the total spin at j site. Our calculation shows that $\Psi_{m=1/2}$ and $\Psi_{m=3/2}$ have the same energy $\frac{J'}{4}$, while $\Psi'_{m=3/2}$ and $\Psi'_{m=1/2}$ are split with $\frac{-J'}{4}$ and $\frac{-J'}{4} - \frac{2J'}{9}$ respectively. These results clearly reveal that the electron favors the lower $|m = \pm 3/2\rangle$ subspace, which gives Q_{z^2} quadrupole states. Notice that, $\pm \frac{\sqrt{3}}{2} Q_{x^2} - \frac{1}{2} Q_{z^2}$ states are equivalent to Q_{z^2} state due to the cubic symmetry, and the orbital frustration still remains.

In order to release the restriction of cubic symmetry and investigate the possible orbital ordering, we further construct the tetragonal supercell with vector $Q=2\pi(001)$ respecting to the cubic unit cell, as shown by the dashes in Fig. 1a, which has been widely reported in double perovskite materials[40–43]. The calculated results in Fig. 2c demonstrate the splitting between Q_{z^2} state (about 8 meV higher) and $\pm \mu Q_{x^2} - \nu Q_{z^2}$ states ($\mu \neq \frac{\sqrt{3}}{2}$ and $\nu \neq \frac{1}{2}$), suggesting that electrons in this system tend to occupy d_{xy} orbital. This result implies that Ba_2MgReO_6 has the easy-plane anisotropy, which has been included in the H_{tb} already. Such anisotropy can be reflected by the occupation in Fig. 2d, which is uniform (1/3) for the three orbitals in the small U regime, but is enhanced to over 0.5 for d_{xy} orbital with U increasing, illustrating the partially breaking of orbital frustration.

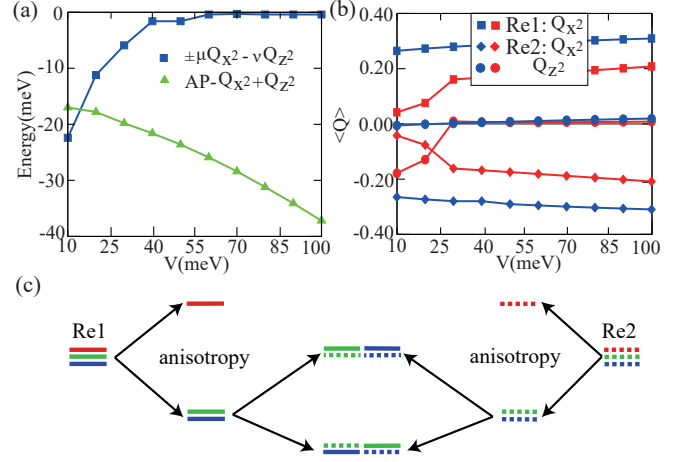


FIG. 3. (a) Total energy of ordering states relative to the cubic as a function of V when $U=1.0\text{eV}$ and $\lambda=0.28\text{eV}$. (b) Evolution of quadrupolar order parameters of AP- $Q_{x^2} + Q_{z^2}$ state with V increasing. Red and blue represent the nonmagnetic and CAF magnetic ground states, respectively. (c) Evolution of orbital ordered states under anisotropy and intersite Coulomb repulsion V in Ba_2MgReO_6 . The solid line on the left and the dotted line on the right represent different Re atoms in tetragonal supercell. Red, green and blue represent Q_{z^2} , $\frac{\sqrt{3}}{2} Q_{x^2} - \frac{1}{2} Q_{z^2}$ and $-\frac{\sqrt{3}}{2} Q_{x^2} - \frac{1}{2} Q_{z^2}$ ordered states, respectively.

In the next, we take the intersite Coulomb repulsion into account with the form $H_V = V \sum_{\alpha} \sum_{\langle ij \rangle \in \alpha} [\frac{4}{3} (n_{i,\beta} - n_{i,\gamma})(n_{j,\gamma} - n_{j,\beta}) + \frac{4}{9} n_{i,\alpha} n_{j,\alpha}]$ ($\alpha=XY, YZ, ZX$), which usually reaches hundreds meV in 5d compounds [44] and is reported to play critical role for the quadrupole arrangement [7]. The energy and orders of quadrupole states versus V are shown in Fig. 3a & 3b with $U = 1.0\text{eV}$ and $\lambda=0.28\text{eV}$. With V increasing, the energy of $\pm \mu Q_{x^2} - \nu Q_{z^2}$ states is soon close to cubic phase, while another new quadrupole state with AP- Q_{x^2} order and small $+Q_{z^2}$ are stabilized.

Such results can be reflected by the electron occupation of Re atoms in AP- $Q_{x^2} + Q_{z^2}$ state with $V=50\text{meV}$, as shown in Fig. 2(d). Compared to the $V=0$ case (solid line), the d_{xy} occupation (dotted red line) is decreased. On the other hand, as shown in Fig. 1a, electron of Re1 tends to occupy d_{xz} orbital (green) while electron of Re2 tends to occupy d_{yz} orbital (blue). Such orbital ordering in AP- $Q_{x^2} + Q_{z^2}$ state can maximally reduce the intersite Coulomb repulsion. As shown in Fig. 2d, since n_{xy} is less than 1/3 at $V=50\text{meV}$, a local positive Q_{z^2} with small magnitude is induced on Re1 and Re2 as shown in Fig. 3b. These results clarify that $|m = \pm 1/2\rangle$ replace $|m = \pm 3/2\rangle$ to become the dominant state when $V > 10\text{meV}$. As a result, the presence of V further removes orbital frustration in cubic and stabilize the quadrupolar ground state AP- $Q_{x^2} + Q_{z^2}$.

The above discussion provides a profound understand-

ing about structural instability and orbital ordering in $\text{Ba}_2\text{MgReO}_6$, as schematically illustrated in Fig. 3c. The onsite Coulomb repulsion and strong SOC jointly induce three degenerate orbital ordering, which can be lifted by spontaneous easy-plane anisotropy or intersite Coulomb repulsion V . The anisotropy induces the local Q_{x^2} with small $-Q_{z^2}$, while V enforces the AP- Q_{x^2} and induces small $+Q_{z^2}$. The V in $\text{Ba}_2\text{MgReO}_6$ is stronger comparing to the energy of anisotropy, finally gives the AP- $Q_{x^2}+Q_{z^2}$ order.

We further calculate the quadrupolar phase diagram based on tetragonal supercell with $\lambda = 0.28\text{eV}$, as shown in Fig. 4a. The phase I without orbital ordering (green) is in small U regime, whereas $U > 0.7\text{eV}$ regime shows phase II with $\pm\mu Q_{x^2} - \nu Q_{z^2}$ orders (blue) for small V , and phase III with AP- $Q_{x^2}+Q_{z^2}$ orders (red) for $V > 10\text{meV}$, which indicates that the anisotropy of $\text{Ba}_2\text{MgReO}_6$ is about 10meV .

The orbital ordering in AP- $Q_{x^2}+Q_{z^2}$ state can drive a special magnetic structure, i.e., canted antiferromagnetic state. We rewrite quadrupole Q_{x^2} using the angular momentum operator $Q_{x^2} = \frac{1}{2}(L_x^2 - L_y^2)$, where $L_x = id_{xz}^\dagger d_{xy} + h.c.$ and $L_y = id_{yz}^\dagger d_{xy} + h.c.$ [9]. Because of AP- Q_{x^2} , the L_x and L_y angular momentum on the two Re atoms are exchanged ($L_{x,y}$ of Re1 \leftrightarrow $L_{y,x}$ of Re2), resulting in the glide mirror symmetry $\{M_{110}|(0, 0, a/2)\}$. Thus, the angular momentums form a canted angle which, as SOC is considered, provides a new mechanism of DM interactions $\sum_{\langle i,j \rangle} D(S_i \times S_j)$ in spin space [45]. This interaction is an intrinsic property of the crystal, and induces the canted antiferromagnetic state(CAF) with [110] easy-axis.

Our self-consistent magnetic calculations confirm that the CAF state is 50meV lower than other magnetic states including FM-Z, FM-X, AFM-Z and AFM-X states, as shown in Fig. 4b at $\lambda = 0.28\text{eV}$ and $V = 0.05\text{eV}$. The result also shows the significant energy difference (about 50meV) between X-orientated and the Z-orientated magnetic states, which is much larger than the typical magnetocrystalline anisotropy energy. Such anomaly may be originated from the distinct quadrupoles and octupoles in the magnetic states with different symmetries.

The CAF state in $\text{Ba}_2\text{MgReO}_6$ exhibits rich magnetic multipole physics including dipoles and octupoles. In Re1, the ratio of $L_x+2S_x(0.258\mu_B)$ to $L_y+2S_y(0.117\mu_B)$ is approximately 2.2 in the CAF ground state, leading to $0.283\mu_B$ magnetic moment with canted angle $\phi \sim 20^\circ$ along [110] direction, which agrees well with the experimentally measured $0.3\mu_B$. In addition, CAF state also has considerable octupoles including $O_{21}^{31}, O_{21}^{33}, O_{21}^{34}$ and O_{21}^{36} . We plot the evolution of octupoles on Re1 with increment of U in Fig. 4c, in which the values of O_{21}^{34} and O_{21}^{36} reduce slowly, whereas O_{21}^{33} increases. By exchange L_x and L_y in the expression of octupoles, we obtain the relationship of the octupoles on the two Re atoms

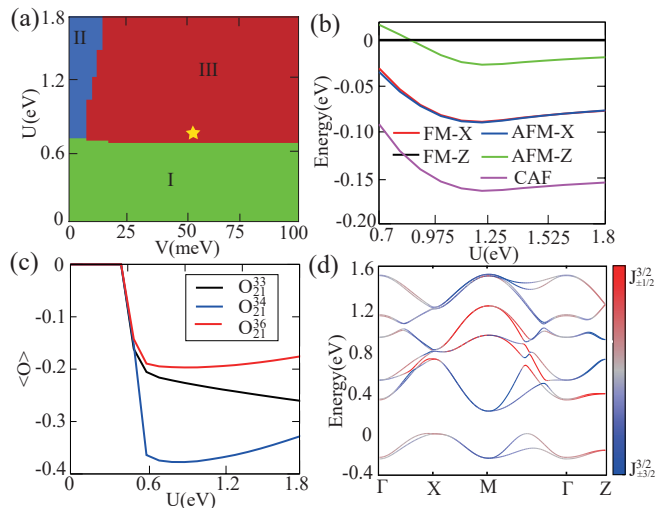


FIG. 4. (a)The quadrupolar ground state phase diagram as a function of U and V . Region I, II, and III represent cubic, $\pm\mu Q_{x^2} - \nu Q_{z^2}$, and AP- $Q_{x^2} + Q_{z^2}$ states, respectively. $\text{Ba}_2\text{MgReO}_6$ is located at the position marked by the yellow star. (b)Total energy of possible magnetic states relative to FM-Z. (c)The magnitude of the addition octupoles in CAF ground state, including O_{21}^{33}, O_{21}^{34} and O_{21}^{36} . (d)Band structures of CAF ground state at $U=0.8\text{eV}$, $V=0.05\text{eV}$.

	O_{21}^{31}	O_{21}^{33}	O_{21}^{34}	O_{21}^{36}
Re1	-	-0.2213	-0.3772	-0.1961
Re2	-0.3772	0.1961	-	0.2213

TABLE I. The weights of magnetic octupoles at $\lambda = 0.28\text{eV}$, $U = 0.8\text{eV}$ and $V = 0.05\text{eV}$ for CAF ground state.

as $O_{21}^{31}(\text{Re1})=O_{21}^{34}(\text{Re2})$ and $O_{21}^{33}(\text{Re1})=-O_{21}^{36}(\text{Re2})$. It reveals that AP- Q_{x^2} makes octupoles also have a canted angle as listed in Table I. Since the magnitude of octupoles is as large as dipole, they should have a significant impact on the electronic structure and physical properties of $\text{Ba}_2\text{MgReO}_6$. How to detect the complex magnetic octupoles is an interesting and important question waiting for addressing in the future.

We also discuss the effect of magnetic orders on quadrupole orders in CAF ground state. Fig. 3b compares the quadrupole order of the non-magnetic and CAF state, in which the weight of Q_{x^2} in the CAF ground state is obviously enhanced. This result illustrates the further enhancement of tetragonal distortion in the magnetic phase, which is consistent with the increment of quadrupoles below T_m reported in experiment [18].

In Fig. 4d, by using $U=0.8\text{eV}$, $\lambda=0.28\text{eV}$ and $V=50\text{meV}$, we obtain the band structures of CAF ground state, which gives rise to a Mott insulating state and the band gap of 0.2eV agree well with the experimental observation (0.17eV [17]). We use these fitted parameters to determine the position of $\text{Ba}_2\text{MgReO}_6$ in the

quadrupolar phase diagram as shown by the yellow star in Fig. 4a, which is close the phase boundary between phase III and phase I. This result implies that possible quantum phase transition may be induced by the substitution, pressure and magnetic field. The projection in Fig. 4d also demonstrates that the occupied bands have more $|J_{eff} = 3/2, m = \pm 1/2 \rangle$ (red) weights than $|J_{eff} = 3/2, m = \pm 3/2 \rangle$ (blue), which confirms our previous analysis again.

In summary, we use the self-consistent unrestricted Hartree-Fock mean-field method to investigate the orbital ordering with the consideration of U, λ and V interactions. The calculation illustrates that U and λ induce the emergence of the orbital orderings as Q_{z^2} and $\pm \frac{\sqrt{3}}{2}Q_{x^2} - \frac{1}{2}Q_{z^2}$, which are equivalent due to the cubic symmetry. The orbital frustration can be partially removed by the easy-plane anisotropy in the tetragonal supercell, leading to more stable $\pm \mu Q_{x^2} - \nu Q_{z^2}$ states. While V is taken into account, Q_{x^2} will be arranged antiparallely, and the Q_{z^2} order gain a small positive magnitude. As a result, the interactions U, λ , V and the anisotropy of $\text{Ba}_2\text{MgReO}_6$ determine it in a AP- $Q_{x^2} + Q_{z^2}$ quadrupolar phase. We reveal that the glide mirror symmetry presented by AP- Q_{x^2} give rise to the CAF magnetic ground state, in which, our calculation found the octupoles $O_{21}^{31}, O_{21}^{33}, O_{21}^{34}$ and O_{21}^{36} . Those octupoles also present canted angle with considerable magnitude. Their possible interesting physical phenomena is an open question for the next study in $\text{Ba}_2\text{MgReO}_6$.

Acknowledgments — The authors thank Yilin Wang, Zhida Song, Jianzhou Zhao, Wenxuan Qiu and Aiyun Luo for valuable discussion. This work was supported by the National Key Research and Development Program of China (2018YFA0307000), and the National Natural Science Foundation of China (12274154).

* These authors made equal contributions to this work.

† e-mail address: gangxu@hust.edu.cn

- [1] B. Kim, H. Jin, S. Moon, J.-Y. Kim, B.-G. Park, C. Leem, J. Yu, T. Noh, C. Kim, S.-J. Oh, *et al.*, *Physical review letters* **101**, 076402 (2008).
- [2] B. Kim, H. Ohsumi, T. Komesu, S. Sakai, T. Morita, H. Takagi, and T.-h. Arima, *Science* **323**, 1329 (2009).
- [3] H. Shinaoka, S. Hoshino, M. Troyer, and P. Werner, *Phys. Rev. Lett.* **115**, 156401 (2015).
- [4] S. M. Disseler, C. Dhital, A. Amato, S. R. Giblin, C. de la Cruz, S. D. Wilson, and M. J. Graf, *Phys. Rev. B* **86**, 014428 (2012).
- [5] A. S. Erickson, S. Misra, G. J. Miller, R. R. Gupta, Z. Schlesinger, W. A. Harrison, J. M. Kim, and I. R. Fisher, *Phys. Rev. Lett.* **99**, 016404 (2007).
- [6] W. Witczak-Krempa, G. Chen, Y. B. Kim, and L. Balents, *Annual Review of Condensed Matter Physics* **5**, 57 (2014).
- [7] G. Chen, R. Pereira, and L. Balents, *Physical Review B* **82**, 174440 (2010).
- [8] G. Chen and L. Balents, *Phys. Rev. B* **84**, 094420 (2011).
- [9] Y. Wang, H. Weng, L. Fu, and X. Dai, *Phys. Rev. Lett.* **119**, 187203 (2017).
- [10] W.-X. Qiu, J.-Y. Zou, A.-Y. Luo, Z.-H. Cui, Z.-D. Song, J.-H. Gao, Y.-L. Wang, and G. Xu, *Phys. Rev. Lett.* **127**, 147202 (2021).
- [11] D. D. Maharaj, G. Sala, M. B. Stone, E. Kermarrec, C. Ritter, F. Fauth, C. A. Marjerrison, J. E. Greedan, A. Paramekanti, and B. D. Gaulin, *Phys. Rev. Lett.* **124**, 087206 (2020).
- [12] J. c. v. Chaloupka, G. Jackeli, and G. Khaliullin, *Phys. Rev. Lett.* **105**, 027204 (2010).
- [13] L. Balents, *Nature* **464**, 199 (2010).
- [14] D. Khomskii and M. Mostovoy, *Journal of Physics A: Mathematical and General* **36**, 9197 (2003).
- [15] T. Takayama, J. Chaloupka, A. Smerald, G. Khaliullin, and H. Takagi, *Journal of the Physical Society of Japan* **90**, 062001 (2021).
- [16] K. G. Bramnik, H. Ehrenberg, J. K. Dehn, and H. Fuess, *Solid state sciences* **5**, 235 (2003).
- [17] D. Hirai and Z. Hiroi, *Journal of the Physical Society of Japan* **88**, 064712 (2019).
- [18] D. Hirai, H. Sagayama, S. Gao, H. Ohsumi, G. Chen, T.-h. Arima, and Z. Hiroi, *Physical Review Research* **2**, 022063 (2020).
- [19] A. M. Tehrani and N. A. Spaldin, *Physical Review Materials* **5**, 104410 (2021).
- [20] S. Lovesey and D. Khalyavin, *Physical Review B* **103**, 235160 (2021).
- [21] J. Pásztorová, A. M. Tehrani, I. Živković, N. A. Spaldin, and H. M. Rønnow, arXiv preprint [arXiv:2210.13616](https://arxiv.org/abs/2210.13616) (2022).
- [22] C. Svoboda, W. Zhang, M. Randeria, and N. Trivedi, *Physical Review B* **104**, 024437 (2021).
- [23] T. Liang, T. H. Hsieh, J. J. Ishikawa, S. Nakatsuji, L. Fu, and N. P. Ong, *Nature Physics* **13**, 599 (2017).
- [24] L. Zhao, D. Torchinsky, H. Chu, V. Ivanov, R. Lifshitz, R. Flint, T. Qi, G. Cao, and D. Hsieh, *Nature Physics* **12**, 32 (2016).
- [25] G. L. Stamokostas and G. A. Fiete, *Physical Review B* **97**, 085150 (2018).
- [26] S. Maekawa, T. Tohyama, S. E. Barnes, S. Ishihara, W. Koshibae, and G. Khaliullin, *Physics of transition metal oxides*, Vol. 144 (Springer Science & Business Media, 2004).
- [27] T. Suzuki, M. Katsumura, K. Taniguchi, T. Arima, and T. Katsufuji, *Phys. Rev. Lett.* **98**, 127203 (2007).
- [28] I. S. Elfimov, V. I. Anisimov, and G. A. Sawatzky, *Phys. Rev. Lett.* **82**, 4264 (1999).
- [29] M. Kargarian, J. Wen, and G. A. Fiete, *Phys. Rev. B* **83**, 165112 (2011).
- [30] K. Kugel and D. Khomskii, *Zh. Eksp. Teor. Fiz* **64**, 1429 (1973).
- [31] G. Kresse and J. Furthmüller, *Phys. Rev. B* **54**, 11169 (1996).
- [32] G. Kresse and J. Furthmüller, *Computational Materials Science* **6**, 15 (1996).
- [33] A. A. Mostofi, J. R. Yates, G. Pizzi, Y.-S. Lee, I. Souza, D. Vanderbilt, and N. Marzari, *Computer Physics Communications* **185**, 2309 (2014).
- [34] A. Georges, L. d. Medici, and J. Mravlje, *Annu. Rev. Condens. Matter Phys.* **4**, 137 (2013).
- [35] H.-T. Jeng, G. Y. Guo, and D. J. Huang, *Phys. Rev.*

- Lett. **93**, 156403 (2004).
- [36] H.-T. Jeng, G. Y. Guo, and D. J. Huang, *Phys. Rev. B* **74**, 195115 (2006).
- [37] S. Sarkar, T. Maitra, R. Valentí, and T. Saha-Dasgupta, *Phys. Rev. Lett.* **102**, 216405 (2009).
- [38] H.-T. Jeng, G. Y. Guo, and D. J. Huang, *Phys. Rev. Lett.* **93**, 156403 (2004).
- [39] H.-T. Jeng, S.-H. Lin, and C.-S. Hsue, *Phys. Rev. Lett.* **97**, 067002 (2006).
- [40] S. Gao, D. Hirai, H. Sagayama, H. Ohsumi, Z. Hiroi, and T.-h. Arima, *Phys. Rev. B* **101**, 220412 (2020).
- [41] K. Yamamura, M. Wakeshima, and Y. Hinatsu, *Journal of solid state chemistry* **179**, 605 (2006).
- [42] A. S. Erickson, S. Misra, G. J. Miller, R. R. Gupta, Z. Schlesinger, W. A. Harrison, J. M. Kim, and I. R. Fisher, *Phys. Rev. Lett.* **99**, 016404 (2007).
- [43] K. E. Stitzer, M. D. Smith, and H.-C. zur Loye, *Solid State Sciences* **4**, 311 (2002).
- [44] O. Nagai and T. Nakamura, *Progress of Theoretical Physics* **24**, 432 (1960).
- [45] H. Katsura, N. Nagaosa, and A. V. Balatsky, *Phys. Rev. Lett.* **95**, 057205 (2005).